Scientific Reports

https://doi.org/10.1038/s41598-026-52921-w

Article in Press

Social processing in the amygdala: single-nucleus RNA-sequencing reveals distinct neuronal responses to dominant and subordinate cues

Received: 9 January 2026

Accepted: 8 May 2026

Published online: 02 June 2026

Cite this article as: Dwortz M.F., Hofmann H.A. & Curley J.P. Social processing in the amygdala: single-nucleus RNA-sequencing reveals distinct neuronal responses to dominant and subordinate cues. *Sci Rep* (2026). https://doi.org/10.1038/s41598-026-52921-w

Madeleine F. Dwortz, Hans A. Hofmann & James P. Curley

Social Processing in the Amygdala: Single-Nucleus RNA-Sequencing Reveals Distinct Neuronal Responses to Dominant and Subordinate Cues

Dwortz, Madeleine F.[1,2,3*], Hans A. Hofmann[1,4], James P. Curley[1,2]

[1] *Interdisciplinary Neuroscience Program, The University of Texas at Austin, Austin, Texas, United States of America*

[2] *Department of Psychology, The University of Texas at Austin, Austin, Texas, United States of America*

[3] *Genomic Sequencing and Analysis Facility, Center for Biomedical Research Support, The University of Texas at Austin, Austin, Texas, United States of America*

[4] *Department of Integrative Biology, The University of Texas at Austin, Austin, Texas, United States of America*

Corresponding author email address: mdwortz@utexas.edu

Abstract

The amygdala serves as a critical neural hub for interpreting social cues, with its distinct subregions and diverse neuronal populations playing specialized roles in processing these signals. Here, we employ single-nucleus RNA sequencing (snRNA-seq) to characterize neuronal responses in the mouse amygdala to olfactory cues associated with social dominance, uncovering distinct activation

patterns within glutamatergic and GABAergic populations. We find that a glutamatergic cluster closely aligned with Slc17a7 (VGLUT1) medial amygdala (MEA) neurons preferentially responds to dominant cues. In contrast, a larger glutamatergic Slc17a6 (VGLUT2) cluster associated with MEA, cortical, and basomedial amygdala neurons exhibits a heightened response to subordinate cues, underscoring the MEA's role in processing social olfactory information. Additionally, a glutamatergic cluster resembling dorsal endopiriform (EPd) neurons responds more strongly to dominant stimuli, supporting the EPd's role in olfactory perception. We also identify a GABAergic cluster with elevated dopamine receptor 2 (Drd2) expression that predominantly responds to dominant cues, consistent with this receptor's role in mediating threat responses. Finally, gene co-expression network analysis links cluster-specific gene expression to distinct biological processes. Together, these findings reveal neuronal and molecular mechanisms underlying social processing of dominance-related olfactory signals, enhancing our understanding of the neural substrates of social behavior.

Keywords: amygdala, social dominance, single-nucleus RNA sequencing, glutamatergic neurons, GABAergic neurons

Introduction

Social perception is a critical neural function for animals living in social groups. The brain's ability to perceive social context, including the presence, identity, and relative status of conspecifics within a group, crucially guides appropriate social behavior, enabling animals to form and maintain strong social relationships (Adolphs 2001, O'Connell and Hofmann 2011, Dwortz et al. 2022). This is especially important in a dominance

hierarchy, a common form of social organization, where the contextually appropriate expression of dominant or subordinate behavior determines an individual's access to resources and chances of survival. Decades of research show that the amygdala is crucial for proper social functioning in dominance hierarchies and that it may be especially important for the perception of dominance cues (Rosvold, Mirsky, and Pribram 1954, Adolphs 2003). For instance, activity in the primate basolateral amygdala (BLA) is positively associated with the dominance status of perceived individuals' faces (Zink et al. 2008; Munuera, Rigotti, and Salzman 2018). In mice, amygdala subregions innervated by olfactory neurons, such as the posteroventral medial amygdala (MEApv), have been shown to increase their activity in response to dominant olfactory cues (W. Lee et al. 2021; Veyrac et al. 2011). Our recent work in mice suggests that similar response patterns extend to dorsal and anteroventral MEA subregions (MEAd, MEAav), BLA, and dorsal endopiriform nucleus (EPd) (Dwortz and Curley 2025). While many specific subregions within the amygdala contribute to processing social cues, the extensive heterogeneity of this brain region suggests that interconnected nuclei and diverse neural processes underpin social perception.

The amygdala is a highly heterogeneous structure, and recent advancements in single-cell profiling technologies have greatly enhanced our understanding and appreciation of its cellular diversity (Swanson and Petrovich 1998; Yu et al. 2023; Hochgerner et al. 2023). The amygdala

contains a diverse array of neuronal cell types, including excitatory principal neurons and inhibitory interneurons. These cell types are intricately modulated by a complex network of neuromodulators, including dopamine (DA) and neuropeptides such as oxytocin (Oxt) and vasopressin (Avp), which play crucial roles in regulating social behaviors and emotional responses (de la Mora et al. 2010; Yao et al. 2017; Arakawa, Arakawa, and Deak 2010; Fadok, Dickerson, and Palmiter 2009; Lee, Lee, and Kim 2017). The expression of Oxt and Avp receptors is particularly prominent in the medial and central nuclei of the amygdala, areas that are key to processing social stimuli (Dębiec 2005; Ferguson et al. 2001; Ferretti et al. 2019). Moreover, the amygdala hosts a variety of projection neurons, including both glutamatergic and GABAergic populations, that connect different nuclei within the amygdala to other brain regions (Janak and Tye 2015; McGarry and Carter 2017; Kita and Kitai 1990; Dong, Petrovich, and Swanson 2001). Accounting for this cellular diversity is critical for elucidating how the amygdala processes social information.

In the present study, we captured the amygdala's response to social dominance cues using single-nucleus RNA-sequencing (snRNA-seq). This method allowed us to simultaneously analyze responses of multiple amygdala subregions and characterize activated neurons at a granular, cell-type-specific level. Specifically, we exposed mid-ranking mice living in dominance hierarchies to urinary cues from familiar dominant and subordinate individuals and then used single-nucleus RNA-sequencing

(snRNA-seq) to measure transcriptional responses of multiple amygdala subregions. Mid-ranking individuals were selected because they are positioned to encounter and evaluate both higher- and lower-status conspecifics, making them well-suited for examining how the brain differentially processes dominant versus subordinate social cues. To characterize activated neurons at a granular, cell-type-specific level we examined the expression of *Homer1*, an immediate early gene (IEG). IEGs are a class of genes that are rapidly and transiently transcribed upon cell membrane depolarization and, therefore, facilitate the identification of activated neurons. We further analyzed neurotransmitter gene expression and mapped neurons to specific amygdala sub-regions with the Allen Brain Cell database to aid in interpreting the functional implications of our findings. We hypothesized that exposure to dominant and subordinate social cues would elicit transcriptionally distinct patterns of neuronal activation across amygdala subregions. Specifically, we expected that dominant social cues would preferentially recruit excitatory neurons within the medial amygdala, reflecting specialized encoding of socially salient olfactory information. Our results confirm the heterogeneity of the amygdala, revealing a significant presence of both glutamatergic and GABAergic neurons, each distinguished by distinct subtypes. Specifically, we observed that glutamatergic VGLUT1 neurons whose transcriptional signatures were most closely aligned with MEA reference profiles exhibited heightened responses to the dominant olfactory cue. We also found that a cluster of

glutamatergic VGLUT2 neurons with profiles matching those in the medial-cortical and basomedial amygdala regions showed a stronger response to the subordinate olfactory cue. This cluster notably co-expressed both *Oxt* and *Avp* preprohormones at relatively higher levels compared to other clusters. Additionally, we found that *Drd2*-expressing striatal-like GABAergic neurons predominantly responded to dominant olfactory cues. These results demonstrate that multiple mechanisms within the amygdala work together to process social cues.

Methods

Subjects and housing

We used 18 male CD-1 mice (*Mus musculus domesticus*) aged 7 to 8 weeks from Charles River Laboratory (Houston, TX, USA). Upon arrival, mice were marked for identification using blue non-toxic markers (Stoelting Co.) and housed in groups of three in standard cages with pine shaving bedding. For the duration of the experiment (25-26 days), subjects were housed in standard cages with pine shaving bedding under a reverse dark–light cycle and provided standard chow and water *ad libitum*. All procedures were approved by the University of Texas at Austin Institutional Animal Care and Use Committee (IACUC; Protocol No. AUP-2019-00338), were performed in accordance with relevant institutional guidelines and regulations, and are reported in accordance with the ARRIVE guidelines.

Behavioral observations and dominance analysis

Groups were observed for one hour each day for the first five days of group housing and then no less than one hour every other day for the remainder of the study, between 11:00 and 17:00 during the dark phase of the reverse light cycle when mice were most active. This sampling strategy was designed to capture the higher frequency of agonistic interactions that typically occur during initial group formation, when dominance hierarchies emerge and stabilize (Williamson et al. 2016). During observation periods, observers used all-occurrence sampling to document fighting, chasing, mounting, submissive postures, and fleeing behaviors, noting winners and losers (see **Table S1** for ethogram). Behavioral scoring and winner/loser assignments were based on the directionality of interactions (i.e., the initiating animal versus the recipient), consistent with established protocols (Williamson et al. 2016). Behavioral data analysis was then conducted in R Studio using the Compete package (Curley 2016). The cumulative wins and losses for each individual over the housing period were compiled into frequency win/loss sociomatrices for each cohort (**Fig S1**). From these sociomatrices, we calculated the Directional Consistency (DC) of dominance interactions, and David's Scores (DS) (de Vries 1995). DC assesses the degree to which all agonistic interactions in a group occur in the direction of the more dominant individual to the more subordinate individual within each relationship. It is equal to (H- L)/(H+L) where H is the frequency of behaviors occurring in the most frequent direction and L is the frequency of behaviors occurring in the least frequent direction within each relationship.

The significance of DC values was evaluated using a randomization test (Leiva, Solanas, and Salafranca 2008). DS provides an individual dominance rating and ranking for each individual in a group, determining the overall success of each individual at winning contests relative to the success of all other individuals. Briefly, it is derived from the proportion of wins and losses of each individual and is corrected for the frequency of agonistic interactions (de Vries 1995). DS above 0 typically reflects that an animal is socially dominant whereas a DS below 0 typically indicates that an animal is socially subordinate. The most dominant and subordinate individuals in each hierarchy had the highest and lowest DS, respectively. The measures of dominance relationships and hierarchy stability were used to guide assignment of mid-ranked subjects to dominant or subordinate urine exposure conditions (see Results and Fig S1 and Table S2 for details).

Urine collection and odor exposures

Urine collection began one week prior to the odor presentations, starting on days 17 and 18 of group housing, and concluded one day before the odor presentations on days 24 and 25. Previous work has shown that urinary chemical signals associated with dominance status change rapidly during hierarchy formation, with major pheromonal differences emerging within the first few days of group housing and becoming extremely pronounced by day 21 of group housing (Lee et al. 2017). The timing of urine collection and exposure in this study was therefore designed to capture well-established and stable status-dependent chemical cues. During this period, animals in

each social group were routinely handled as part of the urine collection procedure to ensure that samples could be obtained from individuals if rank changes occurred. Urine was collected between 7 and 10 am during the light cycle by gently scruffing the mouse, applying a small amount of pressure on the bladder, and collecting deposited urine directly into an Eppendorf tube. Samples were then immediately stored at −80 °C.

On the morning of odor presentations, urine collected over the previous week was thawed on ice and pooled such that each mid-ranked subject was presented with a pooled urine sample derived from either the most dominant or the most subordinate member of its own home cage (n = 3 per condition). Pooled samples remained at room temperature for approximately one hour prior to presentation. All donors were familiar home-cage members, reducing novelty-related confounds. We did not perform chemical normalization (e.g., creatinine or total protein) of pooled urine, thereby preserving compositional differences inherent to urine derived from dominant versus subordinate animals and more closely replicating stimuli as they occur naturally in a group-living environment.

Odor presentations occurred between the hours of 11 am and 1 pm, during the dark phase of the light cycle. Mid-ranked subjects were first transferred to a separate behavioral testing room and placed in an acrylic testing chamber (14.9 cm × 16.8 cm × 17.75 cm) with a thin layer of fresh pine shaving bedding, under dim red lighting conditions. Stimuli were matched by delivery volumes and exposure durations. They habituated to the

chamber for 30 minutes and were then gently scruffed and the experimenter pipetted 15 µl of urine onto the nasal groove. They were then placed back into the chamber, and the experimenter pipetted 1000 µl of urine distributed across the bedding to ensure broad olfactory exposure within the chamber. Subjects remained in the chamber for an additional 30 minutes and were sacrificed by rapid cervical dislocation followed by decapitation. Immediately upon sacrifice, brain tissue was flash-frozen in dry ice-cooled hexanes and stored at -80°C until further processing.

Amygdala microdissection

Brain tissue was transferred to a −20° C cryostat chamber (Leica Microsystems), where it was embedded in OCT and incubated for approximately 30 minutes before amygdala dissection. We used the publicly available Allen Mouse Brain Atlas (Allen Reference Atlas – Mouse Brain, atlas.brain-map.org) to identify and section regions of interest. Four 300 µm slices were made onto glass slides, and the amygdala was dissected bilaterally using sterile surgical blades (approximately slides 65 to 77 of the Allen Mouse Brain Atlas). The amygdalae from each of the three mid-rank subjects per stimulus group (dominant and subordinate stimuli) were pooled into a single 0.2 ml RNAse-free tube and stored at -80°F until further processing.

Nuclei dissociation, library preparation and sequencing

Samples were removed from the -80°C freezer and briefly brought to room temperature. We then isolated nuclei using a procedure adapted from Salem et al. 2024 (Salem et al. 2024). Samples were homogenized in 1.5 ml Nuclei EZ Lysis Buffer (Sigma # NUC101) with 0.2 U/ul RNAse inhibitor (NEB # ML314L) in pre-chilled 2mls KIMBLE Dounce tissue grinders (Sigma Aldrich D8938). Three up-and-down motions of the dounce sufficiently homogenized the samples. Lysate was then filtered through a 35-µm cell strainer and centrifuged at 900 rcf for 5 minutes at 4 °C. The pellet was resuspended in 700 µl of a 25% iodixanol mixture (2% BSA in 1X PBS supplemented with 0.2 U/ul RNAse inhibitor mixed with 60% iodixanol Optiprep medium, Sigma-Aldrich # D1556). This suspension was then layered on top of 700 µl of a 29% iodixanol cushion in a new 1.5 ml tube and centrifuged at 8,000 rcf for 30 minutes at 4°C. Supernatant was discarded and the pellet was resuspended in 150 µl buffer (2% BSA in 1X PBS supplemented with 0.2 U/ul RNAse inhibitor). This suspension was again filtered through a 35-µm cell strainer twice. The final eluent with nuclei was stained with DAPI and the concentration of nuclei was approximated using a Countess Automated Cell Counter (Thermo Fisher Scientific Single nuclei libraries were prepared by the Genomic Sequencing and Analysis Facility at UT Austin using the Chromium Next GEM Single Cell 3’ Kit v3.1 (10× Genomics, PN-1000128) with a target cell count of 10,000 cells. Libraries then were sequenced on a NovaSeq 6000 using an S4 flow cell.

Initial snRNA-seq data processing

We used the Cell Ranger pipeline (10x Genomics) to align raw sequencing data to the mouse genome (GRCm39, Ensembl release 2024-A), perform cell calling, and generate gene-by-cell UMI count matrices. These matrices were then imported into R (RStudio, v4.3.1) and processed using Seurat (v4.3.0.1) (Hao et al. 2024; 2021; Stuart et al. 2019; Butler et al. 2018). We used the Souporcell pipeline (Heaton et al. 2020) to demultiplex each sample pool and identify three putative individuals (**Fig S2a,b**), as well as to detect and remove doublets (**Fig S2c**). Souporcell demultiplexes pooled samples by leveraging genetic variation (single nucleotide polymorphisms, SNPs) present in RNA-seq reads to cluster cells by donor without requiring prior genotype information. Cells are assigned to individual-specific clusters ("singlets"), while droplets containing mixed genetic signals are classified as doublets and excluded. We then filtered each dataset to ensure comparable cell count and quality between samples. Poor-quality nuclei were identified based on mitochondrial DNA content and MALAT1 expression. Using MALAT1, a nuclear-retained non-coding RNA universally expressed across cell types, as a quality control metric is a recommended approach in processing single-cell and single-nucleus data, as low MALAT1 expression is indicative of droplets lacking nuclei (Clarke and Bader 2024). We retained cells with 500–7,000 expressed genes, less than 1% mitochondrial DNA, and log normalized MALAT1 expression greater than 5 (**Fig S3**). Gene counts were normalized with Seurat's NormalizeData

function, which divides by total expression, scales to a common factor (10,000), and applies log transformation (Stuart et al. 2019).

Data integration, clustering and annotation

We integrated the datasets derived from dominant- and subordinate-urine exposed subjects to identify common cell-type clusters using Seurat (**Fig S4**). This integration reduced batch effects and enabled direct comparison of shared cell-type clusters across conditions, facilitating the identification of cellular heterogeneity and accurate cell-type annotation. To ensure that clustering was based on cell-type similarity rather than activation states, we first removed IEGs. Based on existing literature, the following IEGs were excluded: *Btg2, Jun, Egr4, Fosb, Junb, Gadd45g, Fos, Arc, Nr4a1, Npas4, Coq10b, Tns1, Per2, Ptgs2, Rnd3, Tnfaip6, Srxn1, Tiparp, Ccnl1, Mcl1, Dnajb5, Nr4a3, Fosl2, Nptx2, Rasl11a, Mest, Sertad1, Egr2, Midn, Gadd45b, Dusp6, Irs2, Plat, Ier2, Rrad, Tpbg , Csrnp1, Peli1, Per1, Kdm6b, Inhba, Plk2, Ifrd1, Baz1a, Trib1, Pim3, Lrrk2, Dusp1, Cdkn1a, Pim1, Sik1, Frat2, Dusp5, Egr1, Homer1, Bdnf, Nr4a2* (Hochgerner et al. 2023). Next, a set of 2,000 highly variable features was selected to identify consistent patterns of variation across datasets using Seurat's FindVariableFeatures function. We then computed PCA projections, determining the number of principal components based on the point where the explained variance reached an optimal balance. Seurat's FindNeighbors function was then used to calculate the nearest neighbors for each cell, followed by the

FindClusters function to apply the Louvain algorithm and identify clusters of transcriptionally similar cells (**Fig 1a**).

We assigned cell types to the identified clusters using multiple annotation approaches. First, Seurat's FindAllMarkers function was used to identify cluster-specific marker genes. This function uses a Wilcoxon Rank Sum test to compare gene expression levels between each cluster and all other cells and provides Bonferroni-corrected p-values. In particular, this analysis revealed a distinct cluster of blood cells characterized by high expression of *Ttr*, *Hbb-bs*, and *Hba-a1* (Hochgerner et al. 2023). To perform reference-based classification, we applied SingleR with reference datasets from Celldex (Aran et al. 2019) to assign broad cell classes including neurons, astrocytes, oligodendrocytes, endothelial cells, and epithelial cells. We next used ScType (Ianevski et al. 2022) to refine annotations of specific subtypes, such as oligodendrocyte precursor cells (OPCs), based on curated marker databases. Finally, we employed the Allen Brain Cell "Map My Cells" (MMC) tool to achieve finer anatomical resolution and facilitate comparability with future datasets. MMC uses a hierarchical reference-mapping algorithm based on the Allen Brain Atlas to assign nuclei to specific cell types and returns a bootstrapped probability score reflecting assignment confidence (Z. Yao et al. 2023). It should be noted that these assignments indicate transcriptional similarity to reference-defined cell populations and do not constitute definitive anatomical classification.

We examined the results of these various annotation methods in the 10x Loupe Browser (10x Genomics) and assigned cells based on agreement across methods. Cells with conflicting annotations were re-clustered using the full integration and clustering pipeline, enabling the selection of more biologically relevant genes for feature selection. We next analyzed glutamatergic and GABAergic neurons separately, re-running the clustering workflow within each group to resolve finer neuronal subtypes. To identify overexpressed genes associated with each cluster, we again employed Seurat's FindAllMarkers function.

Identifying differentially activated neuronal populations

We aimed to identify differences in neuronal activity between dominant and subordinate stimuli by comparing the proportions of *Homer1*-expressing (*Homer1*$^{+}$) neurons within each glutamatergic and GABAergic cluster for each individual mouse genotype from the sample pools. Previous work from our laboratory using in situ IEG labeling (catFISH) demonstrated that activity-induced expression of the IEG isoform *Homer1a* is selectively associated with social stimulus exposure occurring approximately 30 minutes prior to brain extraction and fixation (Dwortz and Curley, 2025). Given 10x 3' snRNA-seq quantifies gene-level UMIs, we cannot resolve *Homer1a* versus constitutive *Homer1* isoforms; therefore, we interpret gene-level *Homer1* as a proxy for recent activation. Within our dataset we also found that *Homer1* was the most highly expressed IEG in neurons and showed positive correlations with other IEGs (**Fig S6c,d**). Furthermore,

Homer1^{+} nuclei were enriched for cyclic-nucleotide-mediated signaling and postsynaptic processes (**Fig S7**; **Table S10**), consistent with an activated state.

We applied binomial generalized linear mixed-effect models (GLMMs) to evaluate the association between proportions of *Homer1*$^{+}$ neurons and social stimuli, incorporating the total number of cells per cluster per individual as weights to account for varying cell counts across clusters and individual subjects. To explore the functional characteristics of differentially 'activated' cell populations, we analyzed the MMC subclass annotations assigned to each neuronal cluster. We also used a candidate gene approach and examined neurotransmitter gene expression across subclusters. Additionally, we performed differential gene expression analysis between *Homer1*$^{+}$ and *Homer1*$^{-}$ neurons using Seurat's FindAllMarkers function and Gene Ontology (GO) Enrichment analysis to confirm that processes related to cell activation were activated in these nuclei.

Weighted Gene Co-expression Network Analysis

To further contextualize transcriptional programs across GABAergic and glutamatergic neuronal populations, we performed a high-dimensional weighted gene co-expression network analysis (hdWGCNA) to identify modules of co-expressed genes across the integrated dataset (Morabito et al. 2023). These modules represent groups of co-expressed genes (distinct from neuronal clusters, which group cells), identified based on patterns of gene–gene co-variation across cells. Briefly, hdWGCNA constructs a gene

co-expression network by calculating pairwise correlations between genes across cells then clusters genes with similar connectivity patterns into modules using network-based methods. Each module therefore represents a coordinated transcriptional program across cell populations. We selected soft power thresholds of 12 and 10 for glutamatergic and GABAergic nuclei, respectively, and only included genes expressed in at least 5% of nuclei in each cell type. We computed module eigengenes (MEs) using hdWGCNA's ModuleEigengenes function. Within this function, we adjusted for potential sample quality and technical biases by regressing out the influence of total counts per cell, the percentage of mitochondrial genes expressed, and *Malat1* expression. GO enrichment analysis was then conducted using the Enrichr package to determine active biological pathways associated with each module. For each module, the corresponding gene list was queried against the GO:Biological Process, GO:Cellular Component and GO:Molecular Function databases. (Chen et al. 2013). We examined the expression of MEs and pathway activity across neuronal clusters and analyzed the overlap between cluster-specific gene markers and module-associated genes.

Results

Dominance

All six social groups of male mice established dominance hierarchies with a mean Directional Consistency (DC) of 0.752 ± 0.198 (**Fig S1**; **Table S2**).

Although the total number of interactions varied across cohorts, all groups exhibited significant directional consistency (all DC $p \leq 0.001$), indicating stable dominance relationships. The degree of stability and strength of each dominance relationship determined how subjects were assigned a dominant or subordinate stimulus. For instance, in cohort C, the mid-ranking mouse defeated the most dominant individual in nine interactions, resulting in a low DC score of 0.443. However, this mouse consistently defeated the most subordinate individual, indicating a stable dominance relationship with that opponent despite the lower overall interaction frequency. Consequently, the mid-ranking mouse in cohort C received urine from the subordinate animal (see **Fig S1** for stimulus assignments and **Table S2** for full dominance results).

Neuronal diversity within the amygdala

We identified 22,695 nuclei that passed the quality control filters (11,597 cells in the dominant-stimulus sample and 11,098 in the subordinate-stimulus sample) containing 125,267,275 total reads and 33,696 unique genes. These nuclei included neurons, astrocytes, oligodendrocyte precursor cells (OPCs), oligodendrocytes, blood cells, endothelial cells, non-myelinating Schwann cells (NMSCs), and epithelial cells (**Fig 1**; see **Table S3** for list of cell type gene markers). Neurons clustered robustly into glutamatergic (8,489 cells) and GABAergic (6,904 cells) clusters (**Fig 1a**). Ultimately, only a small fraction of unresolved neurons could not confidently be assigned to glutamatergic or GABAergic classes (**Fig 1b**). Glutamatergic

and GABAergic populations were further clustered, and we identified 16 glutamatergic cell clusters (**Fig 2a-d**) and 11 GABAergic cell clusters (**Fig 2e-h**; see **Tables S4 and Table S5** for neuronal cluster marker genes, that is, genes enriched in a given cluster relative to other clusters). Across neuronal clusters, there was some variability in the relative contributions of each genotype by random chance (**Fig S5c,f**).

We observed cluster-specific expression of *Slc17a7* (VGLUT1) and *Slc17a6* (VGLUT2) subtypes among glutamatergic clusters (**Fig 2c**). Specifically, VGLUT2 neurons were more prominent than VGLUT1 in glutamatergic clusters 0 and 6. In contrast, expression of GABAergic marker genes *Gad1* and *Gad2* were uniformly expressed across GABAergic clusters (GABAergic marker gene *Slc32a1* was very lowly expressed in nuclei) (**Fig 2g**).

We also examined the expression of neurotransmitter and receptor genes known to be implicated in social processing across glutamatergic and GABAergic clusters (**Table S6**). *Oxt* and *Avp* preprohormones were expressed across various subclusters (average log normalized expression in glutamatergic nuclei: *Oxt*: 0.0740 ± 0.281, *Avp*:0.218 ± 0.467; GABAergic nuclei: *Oxt*: 0.0798 ± 0.305, *Avp*: 0.223 ± 0.484). In contrast, the expression of neuropeptide receptor genes was generally low across all nuclei, which was not unexpected, given that many neuropeptide GPCR mRNAs are localized to distal processes rather than the nucleus or soma, making them less readily detected in snRNA-seq (Cajigas et al. 2012)

(average log normalized expression in glutamatergic nuclei: *Oxtr*: 0.0181 ± 0.130, *Avpr1a*: 0.000 ± 0.015, *Avpr1b*: 0.000415 ± 0.0181; GABAergic nuclei: *Oxtr*: 0.0205 ± 0.148, *Avpr1a*: 0.001 ± 0.035, *Avpr1b*: 0.000435 ± 0.0211). However, dopamine receptor genes were detectable (average log normalized expression in glutamatergic nuclei: *Drd1*: 0.040 ± 0.19, *Drd2*: 0.0248 ± 0.166; GABAergic nuclei: *Drd1*: 0.055 ± 0.25, *Drd2*:0.0837 ± 0.329), GABAergic cluster 3 exhibited especially prominent *Drd2* expression compared to other clusters (average log normalized expression: 0.523 ± 0.720) (**Table S6**).

To assess the relative prominence of each subtype within clusters we further analyzed the distribution of neurons across distinct neuroanatomical subtypes using the MMC tool (**Fig 3a-d**). Clusters showed enrichment for specific MMC-derived assignments, which were annotated according to their reference brain region and characteristic gene markers. These assignments indicate that nuclei in our dataset closely match transcriptional profiles in the Allen Brain Cell database, but do not establish definitive anatomical localization. Most glutamatergic nuclei were identified as originating from the basolateral (BLA), basomedial (BMA), lateral (LA), and piriform (PA) amygdala populations grouped in the MMC reference as LA-BLA-BMA-PA, which accounted for 27.9% of all glutamatergic nuclei and clustered primarily within clusters Glut 4, 13, 3, 2, and 11. The next most prevalent glutamatergic assignments were medial amygdala (MEA) Slc17a7 neurons (15.6% of all glutamatergic nuclei; primarily Glut 5, 7, and 8),

MEA-cortical amygdala area (CoA)-BMA Ccdc42 neurons (14.1%; largely restricted to Glut 0), layer 2/3 piriform-entorhinal (PIR-ENT) neurons (12.0%; largely restricted to Glut 1), and anterior cortical amygdala area (CoAa)-PAA-MEA Barhl2 neurons (8.3 largely restricted to Glut 6). MMC assignments were made with high confidence, with average assignment probabilities typically exceeding 95% (**Fig. 3c,e**; **Table S7**).

GABAergic nuclei appeared to be comprised of striatal or striatal-like neurons and local inhibitory neurons. The subtype with the highest attributed proportion was striatal pallidal neurons (STR-PAL Chst9), which accounted for 14.6% of all GABAergic nuclei and comprised approximately all (94.6%) of cluster GABA 1. Prominent GABAergic assignments also included central amygdala (CEA)-bed nucleus of the stria terminalis (BST) Six3 Cyp26b1 neurons (8.4% of all GABAergic nuclei; primarily GABA 6), MEA-BST Sox6 neurons (7.2%), CEA-BST Ebf1 Pdyn neurons (6.4%; primarily GABA 4), CEA-anterior amygdala area (AAA)-BST Six3 Sp9 neurons (5.6%; primarily GABA 4 and GABA 0), and somatostatin-positive neurons (SST; 8.2%; primarily GABA 5) (**Fig. 3d,f**; **Table S7**).

Differential activation across neuronal clusters

Consistent with the stimulus timeline, in which stimulus onset occurred approximately 30 min prior to fixation, *Homer1* was the most highly expressed IEG in glutamatergic and GABAergic neurons (**Fig S6a,b**). Pairwise correlations between IEGs were modest in magnitude (generally $|r| < 0.2$), but broadly statistically significant (**Fig S6c,d**), with *Homer1*

showing among the strongest correlations with longer-timescale IEGs such as *Bdnf* (Tao et al., 1998) (**Fig S6c,d**). *Homer1* expression was generally higher among glutamatergic neurons, with the highest expression in glutamatergic cluster 2 (Glut 2) (mean = 1.11 ± 0.84) (**Fig 4a**). Among GABAergic neurons, cluster 3 (GABA 3) exhibited the highest expression (mean = 0.778 ± 0.747) (**Fig 4b**).

To assess whether *Homer1* expression is associated with neuronal activation and to identify additional genes associated with this active state, we compared transcriptional profiles of *Homer1*$^{+}$ and *Homer1*$^{-}$ nuclei (see **Table S9** for full DEG results). We found overexpression of phosphodiesterase (PDE) genes in glutamatergic and GABAergic *Homer1*$^{+}$ cells (**Fig S7a-d**). PDE's control intracellular signaling by catalyzing second messenger cyclic nucleotides, which in turn control receptor-effector coupling, protein-kinase cascades, and transmembrane signal transduction. GO enrichment analysis of these overexpressed genes revealed terms related to "cyclic-nucleotide-mediated signaling" (see **Table S10** for GO analysis results). We specifically observed overexpression of *Pde10a* in both glutamatergic and GABAergic *Homer1*$^{+}$ neurons, along with *Pde4d* in glutamatergic and *Pde7b and Pde1c* in GABAergic *Homer1*$^{+}$ neurons. Additional GO enrichment terms associated with *Homer1*$^{+}$ neurons across both glutamatergic and GABAergic populations also underscored the processes related to post-synaptic activation, such as "regulation of postsynaptic membrane neurotransmitter receptor levels" and "protein

localization to postsynaptic membrane". This is consistent with the established role of *Homer1*$^{+}$ in interacting with excitatory metabotropic glutamate receptors at the postsynaptic density (Xiao et al. 1998; Vazdarjanova et al. 2002). In contrast, genes overexpressed in *Homer1*$^{-}$ nuclei were associated with GO terms related to cell homeostasis, such as "maintenance of location in cell" and "regulation of cellular component size".

We applied general linear mixed-effect models (GLMMs) for binomially distributed data to proportions of *Homer1*$^{+}$ nuclei within each individual mouse genotype and neuronal cluster to determine if there was an association with the social status of the olfactory stimulus. We observed significant differences in the proportion of *Homer1*$^{+}$ nuclei in several glutamatergic and GABAergic clusters, indicating that specific populations respond more to urine derived from either dominant or subordinate donors (**Fig 4c-h**; see **Table S8** for full GLMM results).

Glutamatergic cluster 8 (Glut 8) exhibited significantly greater proportions of *Homer1*$^{+}$ nuclei in response to dominant stimuli compared subordinate stimuli (Sub – Dom: $\beta = -0.583 \pm 0.202$, $P = 0.004$, 95% CI: -0.980, -0.190). Notably, this cluster was annotated by MMC as most similar to excitatory MEA neurons with VGLUT1 marker *Slc17a7*. Within this cluster, 54.8% of nuclei were confidently identified as MEA *Slc17a7* neurons with a 99.0% average probability of assignment accuracy (avg. probability), while MEA-CA-BMA *Ccdc42* neurons constituted 14.3% (avg.

probability = 95.6%) (**Fig 3c**; see **Table S7** for full MMC assignments). Glut 8 also exhibited a small set of marker genes (*Nxph1, Ntng1, Zfp804b, and E130114P18Rik*) enriched relative to other clusters (Table S4), that are broadly associated with synaptic organization and connectivity (Nishimura-Akiyoshi et al. 2007, Petrenko et al. 1996).

Additionally, proportions of *Homer1*$^{+}$ nuclei in glutamatergic cluster 9 (Glut 9) trended higher in response to dominant compared to subordinate stimuli (Sub – Dom: β =-0.410 ± 0.225, P = 0.068, 95% CI: -0.854, 0.028). Glut 9 was the only cluster enriched for dorsal endopiriform neurons (EPd) at 58.6% (avg. probability = 98.2%) (**Fig 3c**). Its marker genes were broadly associated with excitatory projection neurons and axon guidance molecules, such as *Satb2*, *Bcl11a*, and *Foxp2* (Molyneaux et al. 2007; Alcamo et al. 2008; Du et al. 2022) (Table S4).

In contrast, glutamatergic cluster 0 (Glut 0) exhibited significantly greater proportions of *Homer1*$^{+}$ nuclei in response to subordinate stimuli compared to dominant stimuli (Sub – Dom: β = 0.238 ± 0.105, P = 0.024, 95% CI:0.031,0.444). Cluster Glut 0 was most similar transcriptionally to MEA-CA-BMA *Ccdc42* neurons, accounting for 70.5% (avg. probability = 97.8%). (**Fig 3c, Table S7**). It possessed marker genes associated with glutamatergic synaptic and circuit organization (*Adarb2*, *Ntng1*, *Unc13c*, *Grid2*, and *Sema5a*) (Varoqueaux et al. 2002; Pasterkamp and Kolodkin 2003, Traynelis et al. 2010) as well as serotonin receptor *Htr2c* (Table S4). Glut 0 also exhibited elevated expression of *Oxt* and *Avp* preprohormone

transcripts compared to other neuronal clusters. Specifically, it showed the highest *Oxt* preprohormone expression and the second highest *Avp* preprohormone expression (average log normalized expression of *Oxt*: 0.110 ± 0.363 ; *Avp*: 0.316 ± 0.602; **Table S6**).

We also observed stimulus-associated *Homer1*$^{+}$ expression among GABAergic neurons. GABA 3 exhibited significantly greater proportions of *Homer1*$^{+}$ nuclei in response to dominant compared to subordinate stimuli (Sub – Dom: β = -0.341 ± 0.153, P = 0.026, 95% CI: -0.642, -0.041). This cluster exhibited robustly higher *Drd2* expression compared to all other neuronal clusters (**Table S6**) and was enriched for striatal DRD2-expressing neurons (STR D2) based on the MMC analysis (**Fig 3d**). In addition to *Drd2*,this cluster exhibited marker genes involved in dopaminoceptive striatal signaling, such as *Gnal*, *Rgs9*, and *Adcy5* (Rahman et al. 2003; Lee et al. 2002) (Table S5).

We additionally applied hdWGCNA coupled with GO analysis to identify modules of co-expressed genes across neuronal clusters and to further characterize the biological processes associated with cluster- and stimulus-responsive populations. These modules represent groups of genes with coordinated expression patterns across cells. We discovered five modules within glutamatergic neurons and seven within GABAergic neurons (**Fig S8, Fig S9**; see **Table S11** and **Table S12** for module gene assignments).

We focused on stimulus-responsive clusters to relate module activity to social cue processing. Glut 0, which showed a higher proportion of *Homer1*$^{+}$ nuclei in response to subordinate stimuli, exhibited elevated expression of the brown module eigengene (ME) (**Fig S9a,b**) and a significant overlap between this clusters' marker genes and those of the brown module (**Fig S9g**). GO terms associated with this module included "chloride transport" and "regulation of postsynaptic membrane potential" (**Fig S9e**; see **Table S13** for GO analysis results). Glut 9, which showed a trend toward a higher number of *Homer1*$^{+}$ nuclei in response to dominant stimuli, exhibited elevated expression of the green ME (**Fig S9b, Fig S9g**) and terms related to "cell-cell adhesion" and "cell junction assembly" (**Fig S9e**). Glut 8, which exhibited an elevated proportion of *Homer1*$^{+}$ nuclei in response to dominant stimuli, did not exhibit elevated expression of any particular module, although it did share some marker genes with both brown and green modules (**Fig S9g**). GABA 3, which showed a higher proportion of *Homer1*$^{+}$ nuclei in response to dominant stimuli, exhibited elevated expression of the blue ME (**Fig S9c,d)** and a high degree of overlapping marker genes with the blue module (**Fig S9g**). The top GO terms for the blue module were related to cell activation, including "regulation of cation channel activity", "chemical synaptic transmission" and "protein phosphorylation" (**Fig S9f**). Together, these results show that neuronal populations are associated with distinct co-expressed gene

programs and functional profiles, providing a complementary layer of transcriptional organization beyond cluster-defining marker genes.

Discussion

The amygdala serves as a central hub for processing social information and encompasses diverse subregions and neuronal types (Janak and Tye 2015, Li et al. 2017, Adolphs 2003, Hochgerner et al. 2023). In the present study, we employed snRNA-seq to identify specific neuronal populations within the amygdala activated by social urinary olfactory cues. Our analysis revealed distinct clusters of glutamatergic and GABAergic nuclei, each characterized by neurotransmitter systems and enrichment for specific neuroanatomical cell types. The heterogeneity found in our dataset largely corroborates existing amygdala taxonomy revealed by single-cell RNA-seq studies (Hochgerner et al. 2023). This neuronal diversity highlights the need for cell-type-specific analyses of social processing in the brain.

We identified several neuronal clusters that were differentially activated, as indicated by *Homer1* expression, in response to dominant and subordinate urinary olfactory cues under matched volume and exposure conditions. We intentionally did not chemically normalize urine across stimulus donors, as status-related differences in urinary composition constitute the natural sensory signals through which social status is conveyed. Prior work, including studies from our laboratory (Lee et al. 2017), demonstrates that dominant males produce higher concentrations of

specific urinary pheromones such as darcin, SBTs, and farnesenes, which function as status-linked chemosignals (Novotny et al. 1990; Roberts et al. 2010). Thus, neural activation patterns observed here are best interpreted as responses to biologically relevant cues encoding social status. While chemical profiling of urine is beyond the scope of the present study, the identification of status-responsive neuronal populations provides a foundation for future studies linking specific pheromonal components to circuit-level responses. Importantly, because all subjects were exposed to urine stimuli, our design does not isolate neurons responsive to urine per se; rather, it enables direct comparison of neural responses to dominant versus subordinate social cues. Thus, the transcriptional differences observed here are best interpreted as reflecting differential encoding of relative social status, rather than general odor-evoked activation.

We found that Glut 8, a glutamatergic cluster transcriptionally similar to MEA Slc17a7 (VGLUT1) neurons, responded more to dominant stimuli. This finding aligns with our previous work showing that dominant urinary cues elevate c-fos immunoreactivity in the MEApv, a predominantly glutamatergic region (Keshavarzi et al. 2014; W. Lee et al. 2021). The MEA plays a critical role in processing social olfactory cues, acting as a pivotal relay station within the accessory or vomeronasal olfactory pathway, which primarily processes pheromonal cues (Raam and Hong 2021; Kevetter and Winans 1981; Dulac and Wagner 2006). Numerous studies have shown that activity within the MEA responds to socially-relevant olfactory cues (Li et al.

2017; Bergan, Ben-Shaul, and Dulac 2014; Carvalho et al. 2015; Choi et al. 2005). This context strengthens our current finding that Glut 8, as one of the few neuronal clusters that showed stimulus-associated *Homer1* expression, aligns with the MEApv's specific role in social olfactory processing.

Interestingly, we observed an opposite response pattern in cluster Glut 0, where *Homer1+* proportions were higher in subjects presented with subordinate urine. Glut 0 was transcriptionally similar to MEA-CoA-BMA *Ccdc42* neurons. It notably exhibited the marker gene, *Htr2c*, which encodes serotonin receptor 2C (5-HT2C) (Table S4), a neuromodulatory receptor implicated in affective processing and regulation of social behavior (Nautiyal and Hen 2017). Glut 0 also exhibited the highest and second-highest levels of *Oxt* and *Avp* preprohormone expression among all neuronal clusters, respectively. Numerous studies have confirmed the critical role of the oxytocin receptor (OxtR) in the medial amygdala (MEA) for processing social odors and recognizing socially relevant cues (Li et al. 2017; S. Yao et al. 2017). Oxytocin (Oxt) release in the MEA is also implicated in social memory formation (Ferguson et al. 2001). In contrast, the function of vasopressin (Avp) release in the MEA is not as well understood. Similar to OxtR, Avp receptors (Avpr1a and Avpr1b) are essential for social recognition (Albers 2012; Wang et al. 2013) and facilitate social approach behaviors in the MEA (Arakawa, Arakawa, and Deak 2010). Moreover, Avp signaling in the amygdala is linked to aggression promotion (Bosch and

Neumann 2010) and exhibits sexually dimorphic expression influenced by androgens, which may underpin its role in aggression (Tong, Abdulai-Saiku, and Vyas 2021). It is important to note that neuropeptide receptor transcripts appeared at low levels in our dataset, which is expected because many of these mRNAs are enriched in dendrites rather than in the nucleus (Cajigas et al. 2012). Since snRNA-seq isolates nuclear RNA only, it underdetects cytoplasm-localized transcripts (Bakken et al., 2018), and thus whole-cell scRNA-seq studies of the amygdala report higher receptor detection (O'Leary et al, 2020; Hochgerner et al. 2023).

Glut 0 was also one of two glutamatergic clusters that exhibited low VGLUT1 expression and more prominent VGLUT2 expression compared to other clusters. Indeed, VGLUT2 neurons are the primary glutamatergic subtype intermingled with GABAergic neurons in the MEA and biomedical amygdala (BMA), further validating this cluster's MMC annotation (Hochgerner et al. 2023). Along with the observed increase in Glut 8 activity in response to dominant cues, these results imply that VGLUT1 and VGLUT2 expressing neurons in the amygdala may have distinct roles in processing social olfactory signals. One of the key distinctions between VGLUT1 and VGLUT2 transporters lies in their association with different glutamate release patterns. VGLUT1 is associated with a low probability of glutamate release, which is linked to a susceptibility to long-term potentiation (LTP), a process that strengthens synaptic connections and supporting learning and memory; in contrast, VGLUT2 is associated with to

a high probability of glutamate release and is receptive to long-term depression (LTD), a mechanism that weakens synaptic connections and is also important for the refinement of learning and memory circuits. (Fremeau et al. 2004; Park et al. 2019). How these opposing yet complementary mechanisms underlie differential responses to social stimuli remains unclear. One possible explanation is that activation of VGLUT1-positive neurons in response to dominant cues may enhance the memory of these cues, reinforcing the importance of remembering dominant individuals. In contrast, VGLUT2-positive neuron activation in response to subordinate cues may engage LTD-related mechanisms associated with adaptive forgetting, in which weakening synaptic connections serves to selectively reduce the salience of less behaviorally relevant social information and maintain flexibility in ongoing social interactions (Ryan and Frankland 2022). Further research is required to clarify the unique contributions and potential interactions of these spatially proximal but functionally distinct neuronal populations in processing social cues.

We also observed a increase in response to dominant stimuli in the Glut 9 cluster, which exhibited an expression profile similar to EPd neurons. This cluster also expressed marker genes associated with excitatory projection neuron identity and axon guidance molecules (e.g., Satb2, Bcl11a, and Foxp2) (Molyneaux et al. 2007; Alcamo et al. 2008; Du et al. 2022) (Table S4), consistent with a glutamatergic population within the projection-rich EPd region (Watson, Smith, and Alloway 2017). Although

this clusters response to dominant stimuli did not reach statistical significance ($p = 0.068$), this trend is consistent with prior findings showing increased activation of glutamatergic EPd neurons following exposure to socially dominant individuals (Dwortz and Curley 2025). The EPd appears to be multifunctional, interfacing with areas involved in olfaction (e.g., olfactory bulb, medial amygdala, perirhinal cortex), emotional responses (BLA), memory (e.g., entorhinal cortex), and sensorimotor functions (Neafsey, Hurley-Gius, and Arvanitis 1986; Behan and Haberly 1999; Meis et al. 2008; Watson, Smith, and Alloway 2017). Emerging research also suggests that the EPd regulates interoceptive states, given its consistently high baseline activity during exploratory behavior in mice and during slow-wave sleep in humans (Manjila et al. 2024; Ponomarenko, Korotkova, and Haas 2003). Additionally, some have proposed that EPd activation may contribute to conscious odor perception, as evidenced by situations in which human subjects not only detect an odor but also consciously acknowledge its presence (Traub and Whittington 2022). These findings collectively indicate that the EPd may be involved in integrating internal and external states. While the present results should be interpreted cautiously, they suggest that the EPd may be a promising target for future studies of how animals recognize and evaluate relative dominance cues.

We also observed differential activity in specific GABAergic neurons. We identified a GABAergic cluster, GABA 3 characterized by elevated expression of *Drd2*, which closely resembled striatal DRD2-expressing

neurons. This characterization is supported by its gene marker profile, which included genes associated with dopaminergic signaling that are enriched in DRD2-expressing neurons (e.g., *Gnal*, *Rgs9*, and *Adcy5*) (Rahman et al. 2003; Lee et al. 2002) (Table S5). This raises the possibility that our dataset includes dorsal striatal neurons in proximity to the CEA. Alternatively, this cluster could consist of striatal-*like* DRD2-expressing GABAergic neurons identified within the CEA itself (McCullough et al. 2018; McDonald 1982). The significance of DRD2 signaling within the amygdala includes its role in modulating sociability (Ike et al. 2024), risk avoidance and impulsive behaviors (Kim et al. 2018; Casey et al. 2022). Thus, DRD2 activation in response to dominant odors may reflect social vigilance and avoidance of potentially agonistic interactions. Furthermore, polymorphisms in the *Drd2* gene are linked to variations in amygdala activity and emotional responses to visual social cues in humans (Blasi et al. 2009). Given these insights, our findings suggest that activation of amygdala *Drd2* neurons is involved in evaluating socially relevant cues across various sensory modalities.

We lastly performed hdWGCNA coupled with GO analysis to characterize coordinated biological processes in the amygdala and specifically in stimulus-responsive clusters. For example, Glut 0, which showed increased responsiveness to subordinate stimuli and transcriptionally aligned with neurons in the MEA-CoA-BMA region, exhibited elevated expression of a module enriched for genes related to

chloride transport and regulation of postsynaptic membrane potential, suggesting engagement of synaptic signaling processes in this population. Glut 9, which was transcriptionally similar to EPd neurons and trended toward higher responsiveness to dominant stimuli, exhibited elevated expression of the green module, which is enriched for genes associated with cell-cell adhesion and junction assembly, suggesting that these processes may be particularly relevant for this population. In GABA 3, which was transcriptionally aligned with striatal-like DRD2-expressing GABAergic neurons and showed increased responsiveness to dominant stimuli, we observed enrichment of a module associated with genes involved in cell activation, including regulation of cation channel activity, chemical synaptic transmission, and protein phosphorylation. Collectively, these findings indicate that stimulus-responsive neuronal populations are associated with distinct co-expressed gene programs and functional processes, providing insight into the types of molecular pathways that may support social cue processing in the amygdala.

Conclusion

In conclusion, this study illustrates the utility of single-nucleus transcriptomic approaches for studying neural responses to socially relevant sensory cues. We observe stimulus-associated activation patterns in specific neuronal populations. Specifically, two groups of VGLUT1 neurons, with transcriptional profiles aligning with the MEA and EPd,

respectively, respond more to dominant cues. Conversely, VGLUT2 neurons corresponding to the MEA-Coa-BMA region exhibited elevated responses to subordinate cues. The distinct responses of VGLUT1 and VGLUT2 neurons within the MEA region suggest a MEA-centered circuit may play a key role in mediating responses to social cues. Additionally, the increased expression of both *Avp* and *Oxt* preprohormone mRNAs in the MEA-Coa-BMA population underscores the importance of neuropeptide signaling in regulating social perception. Our results also implicate dopamine DRD2 signaling in inhibitory neuron populations in processing social cues. Future studies should expand the number of sequencing samples to replicate our findings. Ongoing advances in single-cell and single-nucleus RNA-sequencing technologies have improved scalability by reducing costs and increasing throughput, thereby facilitating larger and more comprehensive studies (Qu et al. 2023). Complementary spatial and in situ approaches will also be valuable for confirming the anatomical localization and stimulus-associated gene expression patterns of the neuronal populations identified here. Further research should not only confirm these transcriptional responses but also elucidate the causal relationships between olfactory cues and amygdala neuronal activity and circuit function.

References

Adolphs, R. 2001. “The Neurobiology of Social Cognition.” Current Opinion in Neurobiology 11 (2): 231–39. https://doi.org/10.1016/S0959-4388(00)00202-6.

Adolphs, Ralph. 2003. “Is the Human Amygdala Specialized for Processing Social Information?” *Annals of the New York Academy of Sciences* 985 (1): 326–40. https://doi.org/10.1111/j.1749-6632.2003.tb07091.x.

Albers, H.E. 2012. “The Regulation of Social Recognition, Social Communication and Aggression: Vasopressin in the Social Behavior Neural Network.” *Hormones and Behavior*, Oxytocin, Vasopressin and Social Behavior, 61 (3): 283–92. https://doi.org/10.1016/j.yhbeh.2011.10.007.

Alcamo, E. A., L. C., M. Dautzenberg, et al. 2008. “Satb2 Regulates Callosal Projection Neuron Identity in the Developing Cerebral Cortex.” Neuron 57 (3): 364–77. https://doi.org/10.1016/j.neuron.2007.12.012.

Allen Institute for Brain Science (2011). Allen Reference Atlas – Mouse Brain [brain atlas]. Available from atlas.brain-map.org.

Arakawa, H., K. Arakawa, and T. Deak. 2010. “Oxytocin and Vasopressin in the Medial Amygdala Differentially Modulate Approach and Avoidance Behavior toward Illness-Related Social Odor.” *Neuroscience* 171 (4): 1141–51. https://doi.org/10.1016/j.neuroscience.2010.10.013.

Aran, Dvir, A.P. Looney, L. Liu, E. Wu, V. Fong, A. Hsu, S. Chak, et al. 2019. “Reference-Based Analysis of Lung Single-Cell Sequencing Reveals a

Transitional Profibrotic Macrophage." *Nature Immunology* 20 (2): 163–72. https://doi.org/10.1038/s41590-018-0276-y.

Behan, M., and L.B. Haberly. 1999. "Intrinsic and Efferent Connections of the Endopiriform Nucleus in Rat." *Journal of Comparative Neurology* 408 (4): 532–48. https://doi.org/10.1002/(SICI)1096-9861(19990614)408:4<532::AID-CNE7>3.0.CO;2-S.

Bergan, J.F., Y. Ben-Shaul, and C. Dulac. 2014. "Sex-Specific Processing of Social Cues in the Medial Amygdala." *eLife* 3 (June):e02743. https://doi.org/10.7554/eLife.02743.

Blasi, G., L.L. Bianco, P. Taurisano, B. Gelao, R. Romano, L. Fazio, A. Papazacharias, et al. 2009. "Functional Variation of the Dopamine D2 Receptor Gene Is Associated with Emotional Control as Well as Brain Activity and Connectivity during Emotion Processing in Humans." *Journal of Neuroscience* 29 (47): 14812–19. https://doi.org/10.1523/JNEUROSCI.3609-09.2009.

Bosch, O.J., and I.D. Neumann. 2010. "Vasopressin Released within the Central Amygdala Promotes Maternal Aggression." *European Journal of Neuroscience* 31 (5): 883–91. https://doi.org/10.1111/j.1460-9568.2010.07115.x.

Butler, A., P. Hoffman, P. Smibert, E. Papalexi, and R. Satija. 2018. "Integrating Single-Cell Transcriptomic Data across Different Conditions, Technologies, and Species." *Nature Biotechnology* 36 (5): 411–20. https://doi.org/10.1038/nbt.4096.

Cajigas, Iván J., Georgi Tushev, Tristan J. Will, Susanne tom Dieck, Nicole Fuerst, and Erin M. Schuman. 2012. “The Local Transcriptome in the Synaptic Neuropil Revealed by Deep Sequencing and High-Resolution Imaging.” *Neuron* 74 (3): 453–66. https://doi.org/10.1016/j.neuron.2012.02.036.

Carvalho, V.M.A., T.S. Nakahara, L. M. Cardozo, M.A.A. Souza, A.P. Camargo, G.Z. Trintinalia, E. Ferraz, and F. Papes. 2015. “Lack of Spatial Segregation in the Representation of Pheromones and Kairomones in the Mouse Medial Amygdala.” *Frontiers in Neuroscience* 9 (August). https://doi.org/10.3389/fnins.2015.00283.

Casey, E., M.E. Avale, A. Kravitz, and M. Rubinstein. 2022. “Partial Ablation of Postsynaptic Dopamine D2 Receptors in the Central Nucleus of the Amygdala Increases Risk Avoidance in Exploratory Tasks.” *eNeuro* 9 (2): ENEURO.0528-21.2022. https://doi.org/10.1523/ENEURO.0528-21.2022.

Chen E., Tan C., Kou Y., Duan Q., Wang Z., Meirelles G., Clark N., Ma'ayan A. Enrichr: interactive and collaborative HTML5 gene list enrichment analysis tool. BMC Bioinformatics. 2013;14:128. doi: 10.1186/1471-2105-14-128.

Choi, G.B., H. Dong, A.J. Murphy, D.M. Valenzuela, G.D. Yancopoulos, L.W. Swanson, and D.J. Anderson. 2005. “Lhx6 Delineates a Pathway Mediating Innate Reproductive Behaviors from the Amygdala to the

Hypothalamus." *Neuron* 46 (4): 647–60. https://doi.org/10.1016/j.neuron.2005.04.011.

Clarke, Z.A., and G.D. Bader. 2024. "MALAT1 Expression Indicates Cell Quality in Single-Cell RNA Sequencing Data." bioRxiv. https://doi.org/10.1101/2024.07.14.603469.

Curley, James P. 2016. "Compete: Analyzing Social Hierarchies: R Package Version 0.1."

Dębiec, J. 2005. "Peptides of love and fear: vasopressin and oxytocin modulate the integration of information in the amygdala." *BioEssays* 27 (9): 869–73. https://doi.org/10.1002/bies.20301.

Dong, H.W., G.D. Petrovich, and L.W. Swanson. 2001. "Topography of Projections from Amygdala to Bed Nuclei of the Stria Terminalis." *Brain Research. Brain Research Reviews* 38 (1–2): 192–246. https://doi.org/10.1016/s0165-0173(01)00079-0.

Du, Heng, Z. Wang, R. Guo, et al. 2022. "Transcription Factors Bcl11a and Bcl11b Are Required for the Production and Differentiation of Cortical Projection Neurons." Cerebral Cortex 32 (17): 3611–32. https://doi.org/10.1093/cercor/bhab437.

Dulac, C. and S. Wagner. 2006. "Genetic Analysis of Brain Circuits Underlying Pheromone Signaling." *Annual Review of Genetics* 40 (February):449–67. https://doi.org/10.1146/annurev.genet.39.073003.093937.

Dwortz, M.F., J. P. Curley, K. M. Tye, and N. Padilla-Coreano. 2022. “Neural Systems That Facilitate the Representation of Social Rank.” Philosophical Transactions of the Royal Society B: Biological Sciences 377 (1845): 20200444. https://doi.org/10.1098/rstb.2020.0444.

Dwortz, M.F., & Curley, J. P. (2025). Capturing dynamic neuronal responses to dominant and subordinate social hierarchy members with catFISH. *Neuroscience*, *579*, 105–119. https://doi.org/10.1016/j.neuroscience.2025.05.025

Fadok, J.P., T.M.K. Dickerson, and R.D. Palmiter. 2009. “Dopamine Is Necessary for Cue-Dependent Fear Conditioning.” *Journal of Neuroscience* 29 (36): 11089–97. https://doi.org/10.1523/JNEUROSCI.1616-09.2009.

Ferguson, J.N., J. M. Aldag, T.R. Insel, and L.J. Young. 2001. “Oxytocin in the Medial Amygdala Is Essential for Social Recognition in the Mouse.” *The Journal of Neuroscience* 21 (20): 8278–85. https://doi.org/10.1523/JNEUROSCI.21-20-08278.2001.

Ferretti, V., F. Maltese, G. Contarini, M. Nigro, A. Bonavia, H. Huang, V. Gigliucci, et al. 2019. “Oxytocin Signaling in the Central Amygdala Modulates Emotion Discrimination in Mice.” *Current Biology* 29 (12): 1938-1953.e6. https://doi.org/10.1016/j.cub.2019.04.070.

Fremeau, R.T. Jr., K. Kam, T. Qureshi, J. Johnson, D.R. Copenhagen, J. Storm-Mathisen, F.A. Chaudhry, R.A. Nicoll, and R.H. Edwards. 2004. “Vesicular Glutamate Transporters 1 and 2 Target to Functionally

Distinct Synaptic Release Sites." *The Journal of Comparative Neurology* 477 (4): 386. https://doi.org/10.1002/cne.20250.

Hao, Y., S. Hao, E. Andersen-Nissen, W. M. Mauck, S. Zheng, A. Butler, M. J. Lee, et al. 2021. "Integrated Analysis of Multimodal Single-Cell Data." *Cell* 184 (13): 3573-3587.e29. https://doi.org/10.1016/j.cell.2021.04.048.

Hao, Y., T. Stuart, M. H. Kowalski, S. Choudhary, P. Hoffman, A. Hartman, A. Srivastava, et al. 2024. "Dictionary Learning for Integrative, Multimodal and Scalable Single-Cell Analysis." *Nature Biotechnology* 42 (2): 293–304. https://doi.org/10.1038/s41587-023-01767-y.

H., Haynes, A. M. Talman, A. Knights, M. Imaz, D. J. Gaffney, R. Durbin, M. Hemberg, and Mara K. N. Lawniczak. 2020. "Souporcell: Robust Clustering of Single-Cell RNA-Seq Data by Genotype without Reference Genotypes." *Nature Methods* 17 (6): 615–20. https://doi.org/10.1038/s41592-020-0820-1.

Hochgerner, H., S. Singh, M. Tibi, Z. Lin, N. Skarbianskis, I. Admati, O. Ophir, et al. 2023. "Neuronal Types in the Mouse Amygdala and Their Transcriptional Response to Fear Conditioning." *Nature Neuroscience* 26 (12): 2237–49. https://doi.org/10.1038/s41593-023-01469-3.

Ianevski, A., A. K. Giri, and T. Aittokallio. 2022. "Fully-Automated and Ultra-Fast Cell-Type Identification Using Specific Marker Combinations from Single-Cell Transcriptomic Data." *Nature Communications* 13 (1): 1246. https://doi.org/10.1038/s41467-022-28803-w.

Ike, K.G.O., S.J.C. Lamers, S. Kaim, S. F. de Boer, B. Buwalda, J.C. Billeter, and M. J. H. Kas. 2024. “The Human Neuropsychiatric Risk Gene Drd2 Is Necessary for Social Functioning across Evolutionary Distant Species.” *Molecular Psychiatry* 29 (2): 518–28. https://doi.org/10.1038/s41380-023-02345-z.

Janak, P.H., and K.M. Tye. 2015. “From Circuits to Behaviour in the Amygdala.” *Nature* 517 (7534): 284–92. https://doi.org/10.1038/nature14188.

Keshavarzi, S., R.K.P. Sullivan, D. J. Ianno, and P. Sah. 2014. “Functional Properties and Projections of Neurons in the Medial Amygdala.” *Journal of Neuroscience* 34 (26): 8699–8715. https://doi.org/10.1523/JNEUROSCI.1176-14.2014.

Kevetter, G.A., and S.S. Winans. 1981. “Connections of the Corticomedial Amygdala in the Golden Hamster. I. Efferents of the ‘Vomeronasal Amygdala.’” *Journal of Comparative Neurology* 197 (1): 81–98. https://doi.org/10.1002/cne.901970107.

Kim, B., S. Yoon, R. Nakajima, H. J. Lee, H. J. Lim, Y.K. Lee, J.S. Choi, B.J. Yoon, G. J. Augustine, and J.H. Baik. 2018. “Dopamine D2 Receptor-Mediated Circuit from the Central Amygdala to the Bed Nucleus of the Stria Terminalis Regulates Impulsive Behavior.” *Proceedings of the National Academy of Sciences of the United States of America* 115 (45): E10730–39. https://doi.org/10.1073/pnas.1811664115.

Kita, H., and S.T. Kitai. 1990. “Amygdaloid Projections to the Frontal Cortex and the Striatum in the Rat.” *Journal of Comparative Neurology* 298 (1): 40–49. https://doi.org/10.1002/cne.902980104.

Lee, J.H., S. Lee, and J.H. Kim. 2017. “Amygdala Circuits for Fear Memory: A Key Role for Dopamine Regulation.” *The Neuroscientist* 23 (5): 542–53. https://doi.org/10.1177/1073858416679936.

Lee, K.W., J.H. Hong, In Y. Choi, et al. 2002. “Impaired D2 Dopamine Receptor Function in Mice Lacking Type 5 Adenylyl Cyclase.” ARTICLE. Journal of Neuroscience 22 (18): 7931–40. https://doi.org/10.1523/JNEUROSCI.22-18-07931.2002.

Lee, W., A. Khan, and J. P. Curley. 2017. “Major Urinary Protein Levels Are Associated with Social Status and Context in Mouse Social Hierarchies.” *Proceedings of the Royal Society B: Biological Sciences* 284 (1863): 20171570. https://doi.org/10.1098/rspb.2017.1570.

Lee, W., H. N. Dowd, C. Nikain, M. F. Dwortz, E. D. Yang, and James P. Curley. 2021. “Effect of Relative Social Rank within a Social Hierarchy on Neural Activation in Response to Familiar or Unfamiliar Social Signals.” *Scientific Reports* 11 (1): 2864. https://doi.org/10.1038/s41598-021-82255-8.

Li, Y., A. Mathis, B. F. Grewe, J.A. Osterhout, B. Ahanonu, M.J. Schnitzer, V.N. Murthy, and C. Dulac. 2017. “Neuronal Representation of Social Information in the Medial Amygdala of Awake Behaving Mice.” *Cell* 171 (5): 1176-1190.e17. https://doi.org/10.1016/j.cell.2017.10.015.

Manjila, S.B., S. Son, H. Kline, R. Betty, Y. Wu, P. Hyun-Jae, D. Parmaksiz, et al. 2024. “Brain-Wide Connectivity and Novelty Response of the Dorsal Endopiriform Nucleus in Mice.” bioRxiv. https://doi.org/10.1101/2024.09.30.615899.

McCullough, K.M., N.P. Daskalakis, G. Gafford, F.G. Morrison, and K.J. Ressler. 2018. “Cell-Type-Specific Interrogation of CeA Drd2 Neurons to Identify Targets for Pharmacological Modulation of Fear Extinction.” *Translational Psychiatry* 8 (August):164. https://doi.org/10.1038/s41398-018-0190-y.

McDonald, A.J. 1982. “Cytoarchitecture of the central amygdaloid nucleus of the rat.” *Journal of Comparative Neurology* 208 (4): 401–18. https://doi.org/10.1002/cne.902080409.

McGarry, L.M., and A.G. Carter. 2017. “Prefrontal Cortex Drives Distinct Projection Neurons in the Basolateral Amygdala.” *Cell Reports* 21 (6): 1426–33. https://doi.org/10.1016/j.celrep.2017.10.046.

Meis, S., J.R. Bergado-Acosta, Y. Yanagawa, K. Obata, O. Stork, and T. Munsch. 2008. “Identification of a Neuropeptide S Responsive Circuitry Shaping Amygdala Activity via the Endopiriform Nucleus.” *PLOS ONE* 3 (7): e2695. https://doi.org/10.1371/journal.pone.0002695.

Molyneaux, B. J., P. Arlotta, J. R. L. Menezes, and J. D. Macklis. 2007. “Neuronal Subtype Specification in the Cerebral Cortex.” Nature Reviews Neuroscience 8 (6): 427–37. https://doi.org/10.1038/nrn2151.

Mora, M.P. de la, A. Gallegos-Cari, Y. Arizmendi-García, D. Marcellino, and K. Fuxe. 2010. “Role of Dopamine Receptor Mechanisms in the Amygdaloid Modulation of Fear and Anxiety: Structural and Functional Analysis.” *Progress in Neurobiology*, Chemical signaling in the nervous system in health and disease: Nils-Åke Hillarp’s legacy, 90 (2): 198–216. https://doi.org/10.1016/j.pneurobio.2009.10.010.

Morabito, S., F. Reese, N. Rahimzadeh, E. Miyoshi, and V. Swarup. 2023. “hdWGCNA Identifies Co-Expression Networks in High-Dimensional Transcriptomics Data.” *Cell Reports Methods* 3 (6): 100498. https://doi.org/10.1016/j.crmeth.2023.100498.

Munuera, J., M. Rigotti, and C.D. Salzman. 2018. “Shared Neural Coding for Social Hierarchy and Reward Value in Primate Amygdala.” *Nature Neuroscience* 21 (3): 415-23. https://doi.org/10.1038/s41593-018-0082-8.

Nautiyal, K. M., and R. Hen. 2017. “Serotonin Receptors in Depression: From A to B.” F1000Research 6 (February): 123. https://doi.org/10.12688/f1000research.9736.1.

Neafsey, E.J., K. M. Hurley-Gius, and D. Arvanitis. 1986. “The Topographical Organization of Neurons in the Rat Medial Frontal, Insular and Olfactory Cortex Projecting to the Solitary Nucleus, Olfactory Bulb, Periaqueductal Gray and Superior Colliculus.” *Brain Research* 377 (2): 261–70. https://doi.org/10.1016/0006-8993(86)90867-X.

Novotny, M., S. Harvey, and B. Jemiolo. 1990. “Chemistry of Male Dominance in the House Mouse,Mus Domesticus.” Experientia 46 (1): 109–13. https://doi.org/10.1007/BF01955433.

O’Connell, L.A., and H.A. Hofmann. 2011. “The Vertebrate Mesolimbic Reward System and Social Behavior Network: A Comparative Synthesis.” Journal of Comparative Neurology 519 (18): 3599–639. https://doi.org/10.1002/cne.22735.

O’Leary, Timothy P, Kaitlin E Sullivan, Lihua Wang, Jody Clements, Andrew L Lemire, and Mark S Cembrowski. 2020. “Extensive and Spatially Variable Within-Cell-Type Heterogeneity across the Basolateral Amygdala.” *eLife* 9 (September): e59003. https://doi.org/10.7554/eLife.59003.

Park, S.K., J.H. Hong, J.K. Jung, H.G. Ko, and Y.C. Bae. 2019. “Vesicular Glutamate Transporter 1 (VGLUT1)- and VGLUT2-Containing Terminals on the Rat Jaw-Closing γ-Motoneurons.” *Experimental Neurobiology* 28 (4): 451. https://doi.org/10.5607/en.2019.28.4.451.

Pasterkamp, R. Jeroen. 2012. “Getting Neural Circuits into Shape with Semaphorins.” Nature Reviews Neuroscience 13 (9): 605–18. https://doi.org/10.1038/nrn3302.

Petrenko, A. G., B. Ullrich, M. Missler, V. Krasnoperov, T. W. Rosahl, and T. C. Südhof. 1996. “Structure and Evolution of Neurexophilin.” Articles. Journal of Neuroscience 16 (14): 4360–69. https://doi.org/10.1523/JNEUROSCI.16-14-04360.1996.

Ponomarenko, A.A., T.M. Korotkova, and H.L. Haas. 2003. “High Frequency (200 Hz) Oscillations and Firing Patterns in the Basolateral Amygdala and Dorsal Endopiriform Nucleus of the Behaving Rat.” *Behavioural Brain Research* 141 (2): 123–29. https://doi.org/10.1016/s0166-4328(02)00327-3.

Raam, T., and W. Hong. 2021. “Organization of Neural Circuits Underlying Social Behavior: A Consideration of the Medial Amygdala.” *Current Opinion in Neurobiology*, The Social Brain, 68 (June):124–36. https://doi.org/10.1016/j.conb.2021.02.008.

Rahman, Z., J. Schwarz, S. J. Gold, et al. 2003. “RGS9 Modulates Dopamine Signaling in the Basal Ganglia.” Neuron 38 (6): 941–52. https://doi.org/10.1016/S0896-6273(03)00321-0.

Roberts, Sarah A., Deborah M. Simpson, Stuart D. Armstrong, et al. 2010. “Darcin: A Male Pheromone That Stimulates Female Memory and Sexual Attraction to an Individual Male’s Odour.” *BMC Biology* 8 (June): 75. https://doi.org/10.1186/1741-7007-8-75.

Rosvold, H.E., A.F. Mirsky, and K.H. Pribram. 1954. “Influence of Amygdalectomy on Social Behavior in Monkeys.” *Journal of Comparative and Physiological Psychology* 47 (3): 173–78. https://doi.org/10.1037/h0058870.

Ryan, T.J., and P.W. Frankland. 2022. “Forgetting as a Form of Adaptive Engram Cell Plasticity.” *Nature Reviews Neuroscience* 23 (3): 173–86. https://doi.org/10.1038/s41583-021-00548-3.

Salem, N.A., L. Manzano, M.W. Keist, O. Ponomareva, A.J. Roberts, M. Roberto, and R. D. Mayfield. 2024. “Cell-Type Brain-Region Specific Changes in Prefrontal Cortex of a Mouse Model of Alcohol Dependence.” *Neurobiology of Disease* 190 (January):106361. https://doi.org/10.1016/j.nbd.2023.106361.

Stuart, T., A. Butler, P. Hoffman, C. Hafemeister, E. Papalexi, W. M. Mauck, Y. Hao, Marlon Stoeckius, P. Smibert, and R. Satija. 2019. “Comprehensive Integration of Single-Cell Data.” *Cell* 177 (7): 1888-1902.e21. https://doi.org/10.1016/j.cell.2019.05.031.

Swanson, L.W., and G.D. Petrovich. 1998. “What Is the Amygdala?” *Trends in Neurosciences* 21 (8): 323–31. https://doi.org/10.1016/s0166-2236(98)01265-x.

Tao, Xu, Steven Finkbeiner, Donald B. Arnold, Adam J. Shaywitz, and Michael E. Greenberg. 1998. “Ca2+ Influx Regulates *BDNF* Transcription by a CREB Family Transcription Factor-Dependent Mechanism.” *Neuron* 20 (4): 709–26. https://doi.org/10.1016/S0896-6273(00)81010-7.

Tong, W.H., S. Abdulai-Saiku, and A. Vyas. 2021. “Arginine Vasopressin in the Medial Amygdala Causes Greater Post-Stress Recruitment of Hypothalamic Vasopressin Neurons.” *Molecular Brain* 14 (1): 141. https://doi.org/10.1186/s13041-021-00850-2.

Traub, R.D., and M.A. Whittington. 2022. “A Hypothesis Concerning Distinct Schemes of Olfactory Activation Evoked by Perceived versus

Nonperceived Input." *Proceedings of the National Academy of Sciences* 119 (10): e2120093119. https://doi.org/10.1073/pnas.2120093119.

Traynelis, S. F., L. P. Wollmuth, C. J. McBain, et al. 2010. "Glutamate Receptor Ion Channels: Structure, Regulation, and Function." Pharmacological Reviews 62 (3): 405–96. https://doi.org/10.1124/pr.109.002451.

Varoqueaux, F., A. Sigler, J.S. Rhee, et al. 2002. "Total Arrest of Spontaneous and Evoked Synaptic Transmission but Normal Synaptogenesis in the Absence of Munc13-Mediated Vesicle Priming." Proceedings of the National Academy of Sciences 99 (13): 9037–42. https://doi.org/10.1073/pnas.122623799.

Vazdarjanova, A., B. L. McNaughton, C.A. Barnes, P.F. Worley, and J.F. Guzowski. 2002. "Experience-Dependent Coincident Expression of the Effector Immediate-Early Genes *Arc* and *Homer 1a* in Hippocampal and Neocortical Neuronal Networks." *The Journal of Neuroscience* 22 (23): 10067–71. https://doi.org/10.1523/JNEUROSCI.22-23-10067.2002.

Veyrac, A., G. Wang, M.J. Baum, and J. Bakker. 2011. "The Main and Accessory Olfactory Systems of Female Mice Are Activated Differentially by Dominant versus Subordinate Male Urinary Odors." *Brain Research* 1402 (July):20–29. https://doi.org/10.1016/j.brainres.2011.05.035.

Vries, H. de. 1995. “An Improved Test of Linearity in Dominance Hierarchies Containing Unknown or Tied Relationships.” *Animal Behaviour* 50 (5): 1375–89. https://doi.org/10.1016/0003-3472(95)80053-0.

Wang, Y., X. Li, L. Li, and Q. Fu. 2013. “Vasopressin in The Medial Amygdala Is Essential For Social Recognition in The Mouse. | EBSCOhost.” March 1, 2013. https://openurl.ebsco.com/contentitem/gcd:86260643?sid=ebsco:plink:crawler&id=ebsco:gcd:86260643.

Watson, G.D.R., J.B. Smith, and K. D. Alloway. 2017. “Interhemispheric Connections between the Infralimbic and Entorhinal Cortices: The Endopiriform Nucleus Has Limbic Connections That Parallel the Sensory and Motor Connections of the Claustrum.” *The Journal of Comparative Neurology* 525 (6): 1363–80. https://doi.org/10.1002/cne.23981.

Williamson, Cait M., W. Lee, and J. P. Curley. 2016. “Temporal Dynamics of Social Hierarchy Formation and Maintenance in Male Mice.” Animal Behaviour 115 (May): 259–72. https://doi.org/10.1016/j.anbehav.2016.03.004.

Xiao, B., J.C. Tu, R.S. Petralia, J. P. Yuan, A. Doan, C.D. Breder, A. Ruggiero, A. A. Lanahan, R.J. Wenthold, and P. F. Worley. 1998. “Homer Regulates the Association of Group 1 Metabotropic Glutamate Receptors with Multivalent Complexes of Homer-Related, Synaptic

Proteins.” *Neuron* 21 (4): 707–16. https://doi.org/10.1016/S0896-6273(00)80588-7.

Yaguchi, K., S. Nishimura-Akiyoshi, S. Kuroki, T. Onodera, and S. Itohara. 2014. “Identification of Transcriptional Regulatory Elements for Ntng1 and Ntng2 Genes in Mice.” Molecular Brain 7 (1): 19. https://doi.org/10.1186/1756-6606-7-19.

Yao, S., J. Bergan, A. Lanjuin, and C. Dulac. 2017. “Oxytocin Signaling in the Medial Amygdala Is Required for Sex Discrimination of Social Cues.” Edited by Richard D Palmiter. *eLife* 6 (December):e31373. https://doi.org/10.7554/eLife.31373.

Yao, Z., C.T.J. van Velthoven, M. Kunst, M. Zhang, D. McMillen, C. Lee, W. Jung, et al. 2023. “A High-Resolution Transcriptomic and Spatial Atlas of Cell Types in the Whole Mouse Brain.” *Nature* 624 (7991): 317–32. https://doi.org/10.1038/s41586-023-06812-z.

Yu, Bin, Q. Zhang, L. Lin, X. Zhou, W. Ma, S. Wen, C. Li, et al. 2023. “Molecular and Cellular Evolution of the Amygdala across Species Analyzed by Single-Nucleus Transcriptome Profiling.” *Cell Discovery* 9 (February):19. https://doi.org/10.1038/s41421-022-00506-y.

Zink, C.F., Y. Tong, Q. Chen, D. S. Bassett, J. L. Stein, and A. Meyer-Lindenberg. 2008. “Know Your Place: Neural Processing of Social Hierarchy in Humans.” *Neuron* 58 (2): 273–83. https://doi.org/10.1016/j.neuron.2008.01.025.

Acknowledgements: We thank members of the Curley and Hofmann labs for their helpful discussions throughout this work. M.F.D. and J.P.C. were supported by the NIH and H.A.H. was supported by the Reeder Endowed Fellowship in Evolutionary Biology. We also thank the Genomic Sequencing and Analysis Facility in the UT Austin Center for Biomedical Research Support (RRID# SCR_021713) for guidance on sample submission as well as library preparation and sequencing. Computational analyses were performed using the Biomedical Research Computing Facility at UT Austin, Center for Biomedical Research Support (RRID#: SCR_021979).

Author Contributions: M.F.D. and J.P.C. conceptualized the study. M.F.D. performed all experiments, including animal work, brain dissections, nuclei isolation, and bioinformatic analyses. J.P.C. and HA.H. provided guidance on statistical approaches and bioinformatic data analysis and contributed to manuscript editing. All authors reviewed and approved the final manuscript.

Data Availability Statement: All data discussed in this article are included in the supplementary materials. Raw sequencing files and processed gene-count matrices are publicly available through the Gene Expression Omnibus (GEO) under accession number GSE310656.

Funding Details: This work was supported by the National Institutes of Health under Grant 5R21MH132981-02.

Additional Information: The authors declare no competing interests.

Figure Legends

Fig 1. Cell Type Diversity in the Amygdala. a) Uniform Manifold Approximation and Projection (UMAP) plot showing the clustering of 22,695 nuclei in the integrated dataset. Nuclei are color-coded by identified cell types, including astrocytes, blood nuclei, endothelial nuclei, epithelial nuclei, GABAergic neurons, glutamatergic neurons, microglia, oligodendrocytes, oligodendrocyte progenitor nuclei (OPCs), and uncharacterized neurons. Labels reflecting the predominant cell type within each group. This visualization highlights the clustering of transcriptionally similar nuclei by their assigned cell type. b) Pie chart showing the relative abundance of each cell type. Glutamatergic neurons (37.4%) and GABAergic neurons (30.42%) represent the most prevalent types. c) Violin plots display the distribution of expression levels for canonical markers specific to each cell type, supporting nuclei classifications. d) Heatmap showing the expression levels of the top 5 annotated marker genes per cell type, selected based on an average Log2(Fold Change) > 1 and a Bonferonni-adjusted P value < 0.05, across individual nuclei. Normalized Log expression levels are scaled from low (blue) to high (light yellow).

Fig 2. Clustering and Gene Expression Profiles of Glutamatergic and GABAergic Neurons. a, e) UMAP visualizations of glutamatergic (a) and GABAergic (e) neuron clusters. Nuclei are color-coded by cluster identity, with each color representing one of the 15 clusters for glutamatergic neurons and 10 clusters for GABAergic neurons. The clusters represent distinct subpopulations based on gene expression similarities. b, f) Tables

showing the number of nuclei per cluster for glutamatergic (b) and GABAergic (f) neurons, respectively. Each cluster is assigned a unique identifier with the corresponding count of nuclei, providing a quantitative view of the distribution across clusters. c, g) Violin plots depicting the normalized expression levels of marker genes across clusters for glutamatergic (*Slc17a7* and *Slc17a6*) and GABAergic (*Gad1* and *Gad2*) neurons. d, h) Heatmaps showing the normalized expression of top marker genes for glutamatergic (d) and GABAergic (h) clusters. Rows represent genes selected based on an average Log2(Fold Change) > 1 and a Bonferonni-adjusted P value < 0.05. Columns are nuclei, grouped by cluster. Color intensity indicates the expression level, ranging from low (dark blue) to high (light yellow). These heatmaps provide a comprehensive overview of the gene expression landscape, highlighting genetic differences between the identified clusters.

Fig 3. Characterizing Glutamatergic and GABAergic Clusters. a, b) Bar graphs illustrating the counts of nuclei within the top 20 most populous subclasses as identified by the Map My Cells (MMC) method for glutamatergic (a) and GABAergic (d) neurons. These top 20 subclasses account for 95.69% and 91.03% of all glutamatergic and GABAergic neurons, respectively. c, d) Dot plots showing the distribution of neuronal subtypes across the glutamatergic (d) and GABAergic (d) neuron clusters. Dot size indicates the proportion of nuclei in each cluster assigned to the subtype and color intensity reflects the average assignment probability.

Fig 4. Analysis of Immediate Early Gene (IEG) Expression Across Glutamatergic and GABAergic Neuron Clusters. a, b) Violin plots show the distribution of *Homer1* expression across glutamatergic (a) and GABAergic (b) neuron clusters. The mean and medial expression level within each plot is marked by a dot and a star, respectively. c, d) Box plots show the proportion of *Homer1*$^+$ nuclei in response to dominant (Dom) and subordinate (Sub) stimuli across glutamatergic (c) and GABAergic (d) neuron clusters. The significance level of each comparison is indicated in the upper right corner ($p < 0.05$ (*), $p < 0.01$ (**), $p < 0.001$ (***), $0.05 < p < 0.07$ (†). e, f) Volcano plots depict the percentage change in the number of *Homer1*$^+$ nuclei between Dom and Sub stimuli for glutamatergic (e) and GABAergic (f) neuron clusters. Data points represent individual clusters, with the x-axis showing the percentage change and the y-axis indicating the -log10(P value). Points to the right of the vertical dashed line signify significant increases, while those to the left signify decreases. Select clusters discussed in the text are labeled and color-coded according to their cluster identity for visual reference; color does not indicate statistical significance. g, h) Forest plots display the log odds of *Homer1* activation in response to Dom versus Sub stimuli for glutamatergic (g) and GABAergic (h) neuron clusters. Each point on the plot corresponds to the estimate for each cluster, with the horizontal lines representing 95% confidence intervals. Confidence intervals are specified to the right of the plot, followed by the P values. The number of nuclei in each cluster for Dom and Sub

samples, the denominators used to calculate *Homer1*$^{+}$ proportions, are shown to the left of the plot.

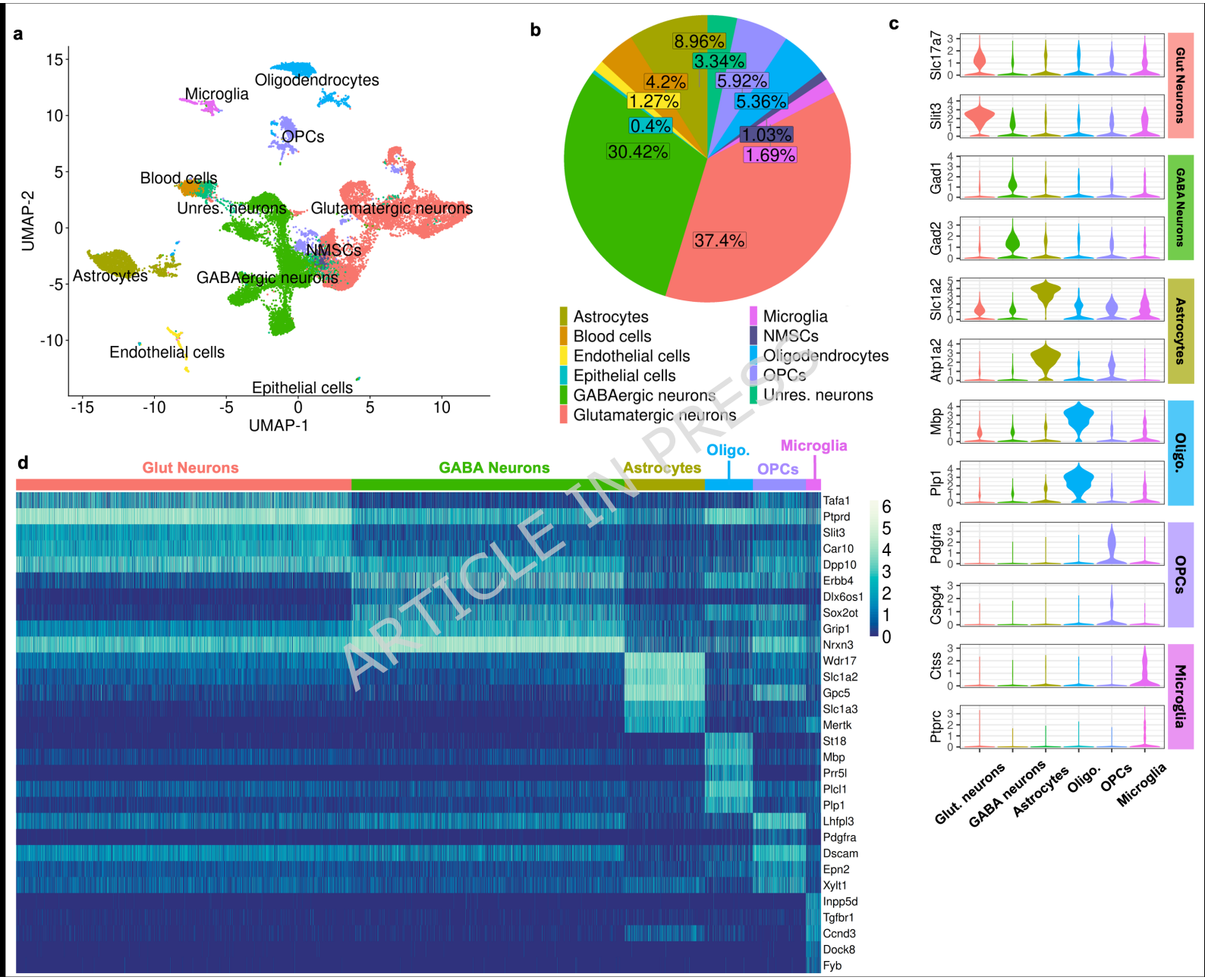

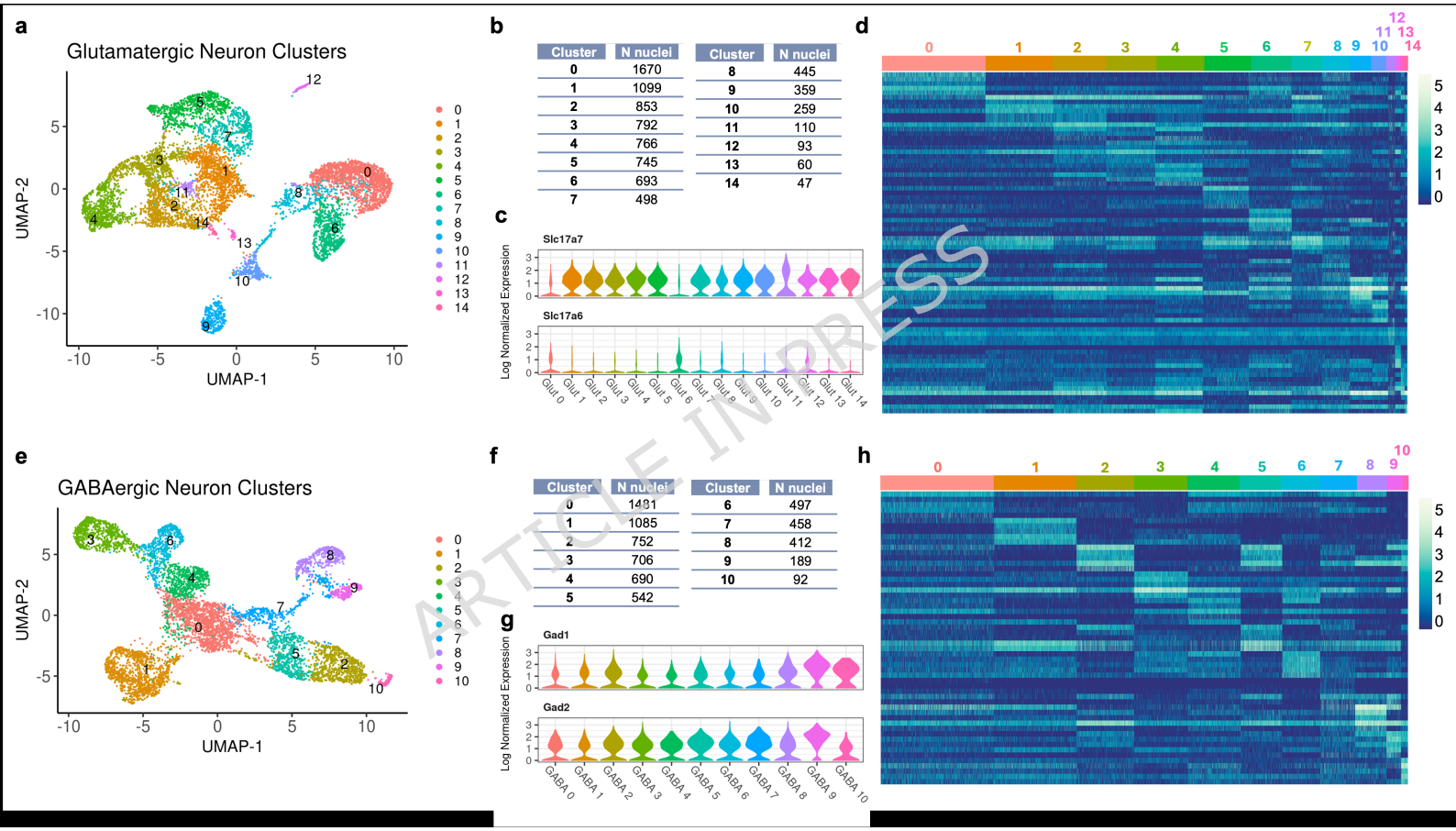

Cluster	N nuclei
0	1670
1	1099
2	853
3	792
4	766
5	745
6	693
7	498
8	445
9	359
10	259
11	110
12	93
13	60
14	47

Cluster	N nuclei
0	1481
1	1085
2	752
3	706
4	690
5	542
6	497
7	458
8	412
9	189
10	92